DØ Note 6082-CONF

Search for Higgs Boson Production in Electron and Muon plus Missing Transverse Energy Final States with 6.7 fb^{-1} of $p\overline{p}$ Collisions at $\sqrt{s} = 1.96$ TeV

The DØ Collaboration
URL http://www-d0.fnal.gov
(Dated: July 20, 2010)

A search for the standard model (SM) Higgs boson is presented using a sample of dilepton events with large missing transverse momentum extracted from 6.7 fb^{-1} of $p\overline{p}$ collisions at $\sqrt{s} = 1.96$ TeV. The final state containing $e^{\pm}\mu^{\mp}$ is considered. The data sample used in this analysis was collected between April 2002 and May 2010 by the DØ detector during Run II of the Fermilab Tevatron collider. No significant excess above background estimations is observed, and upper limits on Higgs boson production are derived, which are 1.35 times the expected SM cross section at M_H=165 GeV.

Preliminary Results for Summer Conferences 2010

I. INTRODUCTION

In the standard model (SM) the masses of the charged fermions are generated by their interaction with a scalar field, the Higgs boson, which has yet to be observed experimentally. The Higgs boson represents the residual degree of freedom after the spontaneous symmetry breaking of the electroweak gauge symmetry $\mathcal{SU}(2) \otimes \mathcal{U}(1)$ which is responsible for the generation of the masses of the W and Z bosons. Direct searches at the CERN e^+e^- collider (LEP) yield a lower limit for the SM Higgs boson mass, $M_H > 114.4$ GeV [1] at 95% confidence level (C.L.). A combination of results from the DØ and CDF experiments excludes the SM Higgs bosons in the mass range $163 < M_H < 166$ GeV at 95% C.L. [2]. Indirect measurements via fits to the electroweak precision data give an upper bound of $M_H < 191$ GeV [3] at 95% C.L. when combined with the direct searches.

In this note, we present a search for the Higgs boson in final states containing a reconstructed electron, a reconstructed muon, and missing transverse energy ($\not\!\!E_T$), using data collected with the DØ detector at the Fermilab Tevatron corresponding to an integrated luminosity of 6.7 fb^{-1}. This final state has good sensitivity for the SM Higgs boson at the Tevatron for $M_H \sim 160$ GeV [4, 5]. Results are presented relative to the sum of the SM predictions for the cross sections of the different Higgs boson production processes, assuming the SM values for the Higgs branching fractions for a range of Higgs boson masses 115-200 GeV. The limits on Higgs boson production obtained in this analysis supersede previous DØ results in the $e^{\pm}\mu^{\mp}$ final state presented in Ref. [6, 7].

II. DØ DETECTOR

We briefly describe the main components of the DØ Run II detector [8] relevant to this analysis. The central tracking system consists of a silicon microstrip tracker (SMT) and a central fiber tracker (CFT), both located within a 2 T axial magnetic field. The SMT strips have a typical pitch of 50–80 μm, and the design is optimized for tracking and vertexing over the pseudorapidity range $|\eta| < 3$, where $\eta = -\ln(\tan\theta/2)$ with θ being the polar angle relative to the proton beam direction. The system has a six-barrel longitudinal structure, with each barrel a set of four silicon layers arranged axially around the beam pipe, interspersed with sixteen radial disks. In addition, a new layer of silicon (Layer 0) was added just outside the beam pipe in 2006. The CFT has eight thin coaxial barrels, each supporting two doublets of overlapping scintillating fibers of 0.835 mm diameter, one doublet parallel to the beam axis, the other alternating by $\pm 3^\circ$ relative to the beam axis.

A liquid-argon/uranium calorimeter surrounds the central tracking system and consists of a central calorimeter (CC) covering to $|\eta| \approx 1.1$, and two end calorimeters (EC) extending coverage for $|\eta| < 4.2$, each housed in separate cryostats. Scintillators between the CC and EC cryostats provide sampling of showers for $1.1 < |\eta| < 1.4$.

The muon system is located outside the calorimeters and consists of a layer of tracking detectors and scintillation trigger counters inside toroid magnets which provide a 1.8 T magnetic field, followed by two similar layers behind each toroid. Tracking in the muon system for $|\eta| < 1$ relies on 10 cm wide drift tubes, while 1 cm mini-drift tubes are used for $1 < |\eta| < 2$. The numbers of hits in the wire chambers and in the scintillators of the the muon spectrometer are combined to define a muon quality variable, used in the final stage of the analysis.

Trigger and data acquisition systems are designed to accommodate the high luminosities of Run II. Based on preliminary information from tracking, calorimetry, and muon systems, the output of the first level of the trigger is used to limit the rate for accepted events to ≈ 1.5 kHz. At the next trigger stage, with more refined information, the rate is reduced further to ≈ 0.8 kHz. These first two levels of triggering rely mainly on hardware and firmware. The third and final level of the trigger, with access to all the event information, uses software algorithms and a computing farm, and reduces the output rate to ≈ 100 Hz, which is written to tape.

III. DATA AND MONTE CARLO SAMPLES

The data sample used in this analysis was collected between April 2002 and May 2010 (Run II) by the DØ detector at the Fermilab Tevatron collider at $\sqrt{s} = 1.96$ TeV, and corresponds to an integrated luminosity of 6.7 fb^{-1} for the $e^{\pm}\mu^{\mp}$ final state. The luminosity is measured with an accuracy of 6.1% using plastic scintillator arrays located in front of the EC cryostats, covering $2.7 < |\eta| < 4.4$ [9]. In order to reproduce the efficiencies measured in data in the $e^{\pm}\mu^{\mp}$ final state, the entire $M_{e\mu}$ spectrum is compared with the $Z/\gamma^* \to \ell\ell$ prediction considering the effect of the τ branching ratios to electrons and muons. The yield of Z candidates observed in data is consistent with the measurement of the luminosity within 5%, after accounting for trigger efficiencies (see Sec. IV).

Signal and SM background processes are simulated with PYTHIA [10] or ALPGEN [11] using the CTEQ6L1 [12] parton distribution functions (PDF), followed by a detailed GEANT-based [13] simulation of the DØ detector. Various Higgs boson production channels contribute to the total signal. The main production channel is the gluon fusion

process $gg \to H \to WW^* \to \ell\nu\ell\nu$, followed by ZH and WH production and then vector–boson fusion process (VBF) $q\bar{q} \to q\bar{q}H \to qqWW^* \to qq\ell\nu\ell\nu$. Decays of the Higgs boson to a pair of Z bosons (and subsequent decay of the Z bosons to leptons, jets, or neutrinos) are also considered. The signal cross sections are normalized to NNLO calculations [14–17] (NLO calculations in the case of the vector boson fusion process) and the distribution of the transverse momentum of the Higgs boson generated in the gluon fusion process is reweighted to match the MC@NLO prediction [18].

The main background processes for this analysis are diboson production, Z/γ^* decays in leptonic final states, electroweak $W + jets/\gamma$ production, $t\bar{t}$ decays and multijet production with jets misidentified as leptons. For the W(+jets) and Z(+jets) backgrounds we use the ALPGEN [11] event generator. The background MC samples for inclusive W and Z production are normalized using the NNLO cross sections calculations of Ref. [19] using the NLO CTEQ 6.1 PDF. The Z boson $p_{\rm T}$ distribution is modeled to match the distribution observed in data [20], taking also into account the dependence on the number of reconstructed jets. To reproduce the W $p_{\rm T}$ distribution in simulated events, the product of the measured Z boson $p_{\rm T}$ spectrum in Ref. [20] multiplied by the ratio of W to Z boson $p_{\rm T}$ distributions at NLO from Ref. [21] is used to reweight events. The NNLO calculations of Ref. [22] are used for $t\bar{t}$ production, while the NLO WW, WZ and ZZ production cross section values are taken from Ref. [23]. For the main source of background, WW production, the $p_{\rm T}$ of the diboson system is modeled using the SHERPA simulation [24] and the distribution of the opening angle of the two leptons is corrected to take into account the contribution from gluon fusion [25]. The background due to multijet production, where jets are misidentified as leptons, is determined from data. The contribution is determined from a sample of events with inverted lepton quality cuts, corrected to match the normalization and kinematics determined in the like-sign data.

IV. EVENT PRESELECTION

All events satisfying any trigger of the DØ trigger suite are accepted for this analysis. While most events selected in the analysis are triggered by single-lepton and dilepton triggers, additional acceptance is gained by including triggers with jets or missing transverse energy. A data-derived correction is derived in a Drell-Yan dominated sample and applied to the simulated samples to account for the effect of the trigger on total yield and kinematic bias. After applying the trigger correction, the simulated background samples are normalized to the integrated luminosity and cross section (NNLO for $W/Z + jets$, and NLO for all other backgrounds) with the predicted yield agreeing with the selected dilepton data to better than the uncertainty on the luminosity (6.1%).

In the offline analysis, electrons are identified using calorimeter and tracking information. Electromagnetic showers are identified in the calorimeter by comparing the longitudinal and transverse shower profiles to those of simulated electrons. The showers must be isolated, deposit 90% of their energy in the electromagnetic part of the calorimeter and pass a likelihood criterion that includes a spatial track match and, in the central detector region, an E/p requirement for central cryostat electrons, where E is the energy of the calorimeter cluster and p is the momentum of the track. Electrons are required to be in the acceptance of the calorimeter.

Muon tracks are reconstructed from hits in the wire chambers and scintillators in the muon system and must match a track in the central tracker. To select isolated muons, the scalar sum of the transverse momentum of all tracks, other than that of the muon, in a cone of $\mathcal{R} = 0.5$ around the muon track is calculated, where $\mathcal{R} = \sqrt{(\Delta\phi)^2 + (\Delta\eta)^2}$ and ϕ is the azimuthal angle. The transverse energy deposited in the calorimeter in a hollow cone of $0.1 < \mathcal{R} < 0.4$ around the muon is also measured. Both quantities are required to be $< 0.15 \times p_{\rm T}^{\mu}$, where $p_{\rm T}^{\mu}$ is the transverse momentum of the muon. Muons are restricted to the fiducial coverage of the muon system $|\eta| < 2.0$. Muons from cosmic rays are rejected by requiring a timing criterion on the hits in the scintillator layers as well as applying restrictions on the position of the muon track with respect to the selected primary vertex.

In all events, two leptons originating from the same position (within 2 cm) along the beamline are required to be of opposite charge. The muon must have $p_T^{\mu} > 10$ GeV while the electron is required to have $p_{\rm T}^{e} > 15$ GeV. This stage of the analysis is referred to as "preselection". Figure 1 shows the dilepton invariant mass and missing transverse energy distributions at preselection.

In order to improve the sensitivity of the analysis, the preselection sample is further subdivided by the number of jets present in the event. Jets are required to have $p_{\rm T} > 15$ GeV, $|\eta| < 2.4$, pass quality requirements, and to have charged tracks associated to the event vertex. The subsequent analysis steps are then carried out for events with zero jets, one jet, and two or more jets. Dividing the analysis into different jet bins significantly increases the sensitivity of the analysis as the signal production composition changes considerably between each sample. Separating according to jet multiplicity allows the multivariate techniques (described below) to better discriminate between signal and background.

The number of events in each jet multiplicity at preselection can be found in TableI. In general, good agreement between data and the expected background contribution is observed. The largest relative discrepancy is observed in

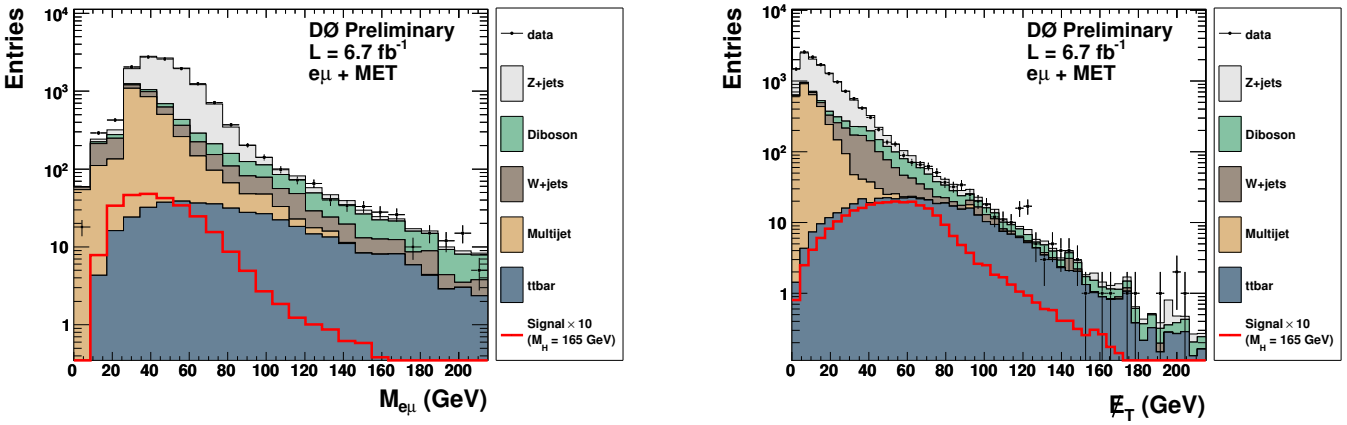

FIG. 1: Distributions of $e^{\pm}\mu^{\mp}$ mass (left) and $\not\!\!E_T$ (right) for data (points with error bars), background simulation (histograms, complemented with the QCD expectation) and signal expectation for $M_H = 165$ GeV (solid line) after preselection.

	Data	Signal	Total Background	$Z \to ee$	$Z \to \mu\mu$	$Z \to \tau\tau$	$t\bar{t}$	$W + jets$	WW	WZ	ZZ	Multi-jet
0 jets	9901	14.1	9988±909	56.5	466.0	5717	11.4	823.6	540.6	19.0	3.5	2351
1 jet	2402	8.5	2292±180	18.9	79.6	1169	114.7	178.0	116.2	7.7	2.2	605.0
$\geq$ 2 jets	924	5.2	828±80	4.6	26.1	239.2	323.4	44.5	24.7	3.3	2.0	160.2

TABLE I: Expected and observed number of events in each jet multiplicity after preselection. The signal assumes a Higgs boson mass of 165 GeV. The error on the total background expectation represents the systematic uncertainty.

the 2 jet channel, where 828 events are expected, while 924 events are observed in the data. Taking all systematic uncertainties into account (see Sec. VI), the systematic uncertainty on the background expectation is roughly 80 events, thus the difference in events expected and observed corresponds to a deviation of slightly more than one σ.

After the $e^{\pm}\mu^{\mp}$ preselection, the Z/γ^* contribution is the dominant background source. For the signal, large missing transverse energy is expected due to neutrinos in the final state, while Z/γ^* events are expected to peak at lower values. Thus, requiring missing transverse larger than 20 GeV rejects the majority of Z/γ^* events. The missing transverse energy distribution at preselection can be found in Fig. 1. The number of events remaining after requiring $\not\!\!E_T > 20$ GeV is shown in Table II.

V. FINAL DISCRIMINANTS

After rejecting the majority of the Z/γ^* background by requirements on the missing transverse energy, the signal is separated from the remaining background using a multivariate technique known as a random forest decision tree (DT). This is a machine learning technique that is used to discriminate signal and background events based on event kinematics. For events with no jets, the variables used in the DT are:

- leading lepton p_T;
- second leading lepton p_T;

	Data	Signal	Total Background	$Z \to ee$	$Z \to \mu\mu$	$Z \to \tau\tau$	$t\bar{t}$	$W + jets$	WW	WZ	ZZ	Multi-jet
0 jets	2662	13.2	2838±224	8.9	172.2	1318	10.8	684.2	447.0	16.5	2.2	177.8
1 jet	1164	7.9	1132±91	4.8	40.6	585.5	107.6	147.6	99.0	6.5	1.6	138.4
$\geq$ 2 jets	636	4.8	594±58	2.3	14.4	162.8	300.6	38.1	21.9	2.7	1.4	49.2

TABLE II: Expected and observed number of events in each jet multiplicity after cutting on the missing transverse energy larger than 20 GeV. The signal assumes a Higgs boson mass of 165 GeV. The error on the total background expectation represents the systematic uncertainty.

- invariant mass of the leading and second leading lepton;
- azimuthal opening angle between the two leading leptons, $\Delta\phi(\ell,\ell)$;
- opening angle in η and ϕ space between the two leading leptons, $\Delta R(\ell,\ell)$;
- $\not\!\!E_T$;
- $\not\!\!E_T^{\rm special}$, where $\not\!\!E_T^{\rm special} = \not\!\!E_T$ if $\Delta\phi(\not\!\!E_T$, nearest lepton or jet) $> \pi/2$ or $\not\!\!E_T^{\rm special} = \not\!\!E_T \times \sin(\Delta\phi(\not\!\!E_T$, nearest lepton or jet) otherwise ;
- minimum of transverse mass between $\not\!\!E_T$ and each lepton, $M_T^{\rm min}$;
- minimum of azimuthal angle between $\not\!\!E_T$ and each lepton;
- maximum of azimuthal angle between $\not\!\!E_T$ and each lepton;
- transverse mass between $\not\!\!E_T$ and dilepton pair, $M_T(\ell\ell, \not\!\!E_T)$;
- electron shower profile likelihood;
- number of Layer 0 hits of the electron candidate;
- muon quality;

For events with one jet, all the zero-jet variables are used, as well as:

- $\not\!\!E_T^{\rm Scaled} = \not\!\!E_T / \sqrt{\sum_{\rm jets} \left(\Delta E^{\rm jet} \cdot \sin\theta^{\rm jet} \cdot \cos\Delta\phi\,({\rm jet}, \not\!\!E_T)\right)^2}$;
- leading jet p_T;
- azimuthal angle between $\not\!\!E_T$ and the leading jet;
- maximum b-tag mva output

Events with two or more jets also use all the zero-jet variables, in addition to:

- leading jet p_T;
- second leading jet p_T;
- absolute value of the pseudo-rapidity difference between the jets, $\Delta\eta(j1, j2)$;
- minimal azimuthal angle between $\not\!\!E_T$ and either the leading or second leading jet;
- maximal azimuthal angle between $\not\!\!E_T$ and either the leading or second leading jet;
- invariant mass of the leading and second leading jet;
- four-body invariant mass of the two leading jets and two leading leptons;
- maximum b-tag mva output;

Simulated events are used to train the DT to differentiate between all Higgs boson signal events, including gluon fusion, associated production and vector boson fusion, and all background events (diboson, top, W boson, Z/γ^*, etc.). The result of this training is a per-event discriminant value with values near zero corresponding to background-like events and values near one corresponding to signal-like events. A separate DT is trained for each of the three jet multiplicities (0, 1, and $\geq$2 jet bins), and for each Higgs boson mass considered. The resulting DT discriminant for the separate channels for a Higgs boson mass of 165 GeV can be found in Fig. 2.

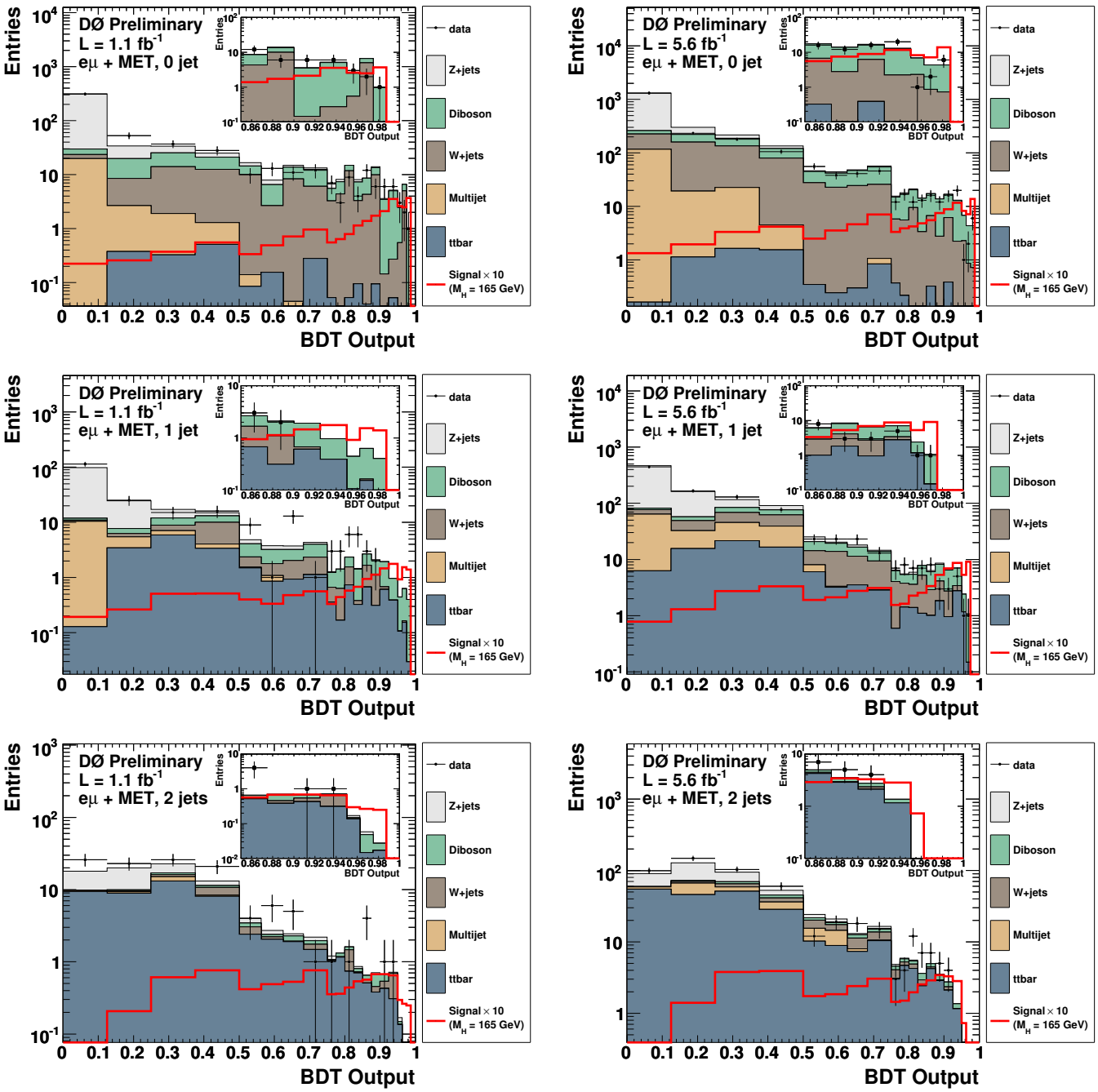

FIG. 2: Final DT discriminant for the $e^{\pm}\mu^{\mp}$ channel for events with no jets (top), one jet (middle), two or more jets (bottom). The left column shows the Run IIa dataset, while the right column is for Run IIb data. The discriminant is for an assumed Higgs mass of 165 GeV.

VI. RESULTS AND SUMMARY

The estimates for the expected number of background and signal events depend on numerous factors that each introduce a systematic uncertainty. We consider the effect of systematic uncertainties both on the normalization and on the shape of the decision tree's differential distributions for signal and backgrounds. The following sources of systematic uncertainties affecting only the normalization of the backgrounds and of the signal efficiency have been considered: lepton reconstruction efficiencies (2.5-4%), lepton momentum calibration (2-8%), theoretical cross section (diboson 7%, $t\bar{t}$ 10%, W+jet 6%, Z+jet 6%), Higgs signal PDFs (8%) and QCD scale (α_s) (8%), modeling of

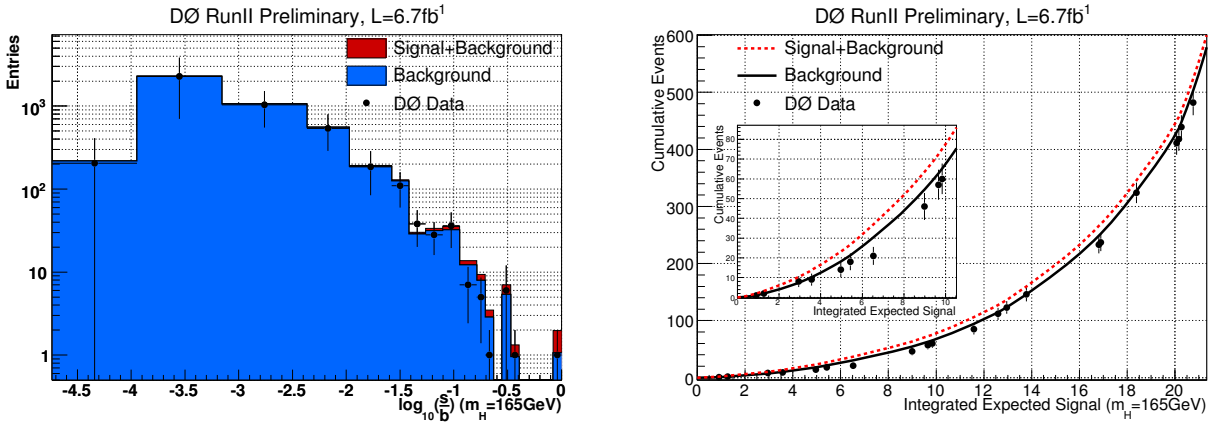

FIG. 3: Distribution of $\log_{10}(s/b)$ (left) and integrated s/b distribution (right) for the background-only and signal+background hypothesis. Both distributions are shown for a Higgs boson mass of 165 GeV.

TABLE III: Expected and observed upper limits at 95% C.L. for $\sigma(p\overline{p} \to H + X)$ relative to the SM for $e\mu$ candidates in Run II for different Higgs boson masses (M_H).

M_H=	115	120	125	130	135	140	145	150	155	160	165	170	175	180	185	190	195	200
$e\mu$ (exp.)	15.32	9.69	7.20	5.33	4.30	3.65	3.19	2.71	2.33	1.76	1.62	1.91	2.22	2.60	3.09	4.05	4.56	5.38
$e\mu$ (obs.)	30.92	22.67	13.82	9.11	5.44	4.64	3.58	2.55	2.06	1.61	1.39	1.57	1.82	2.48	3.46	3.94	4.53	5.66

multijet background (10%), and luminosity (6.1%). For the following source of systematic uncertainties we consider also the impact on the shape the DT distributions: jet reconstruction efficiency (6-18%), jet energy scale calibration (3-17%), jet energy resolution (2%), modeling of $p_{\rm T}(WW)$, $p_{\rm T}(H)$, and $p_{\rm T}(Z)$ (1-5%). The systematic uncertainty on the W and Z boson $p_{\rm T}$ modeling is determined by comparing the $p_{\rm T}$ distributions of ALPGEN to the measured $p_{\rm T}$ distributions in data. The total uncertainty on the background level is approximately 10% and for the signal efficiency it is 13%.

A good way to visualize the sensitivity of the analysis and to show the agreement with the background-only or signal+background hypothesis is to aggregate the predictions and the data in bins of s/b. This also allows to combine the different channels without any loss in sensitivity. Due to the large range in s/b it is more convenient to use $\log_{10}(s/b)$. For a Higgs boson mass of 165 /GeV, the $\log_{10}(s/b)$ distribution for a combination of all jet bins is shown in Fig. 3 (left). Integrating this distribution from the high s/b side downwards shows the background-only and the signal+background hypothesis compared to data in the most sensitive region. This can be seen in Fig. 3 (right), again for a Higgs boson mass of 165 GeV.

After all selection cuts, the DT output distributions in data agree within uncertainties with the expected backgrounds as shown in Figure 2. Thus the DT output distributions are used to set limits on the Higgs boson inclusive production cross section $\sigma(p\overline{p} \to H + X)$ assuming SM values for the branching ratios. We calculate limits using a modified frequentist method, the CLs method, with a log-likelihood ratio (LLR) test statistic [26]. To minimize the degrading effects of systematics on the search sensitivity, the individual background contributions are fitted to the data observation by maximizing a profile likelihood function for each hypothesis [27].

Table III presents expected and observed upper limits at 95% C.L. for $\sigma(p\overline{p} \to H + X)$ relative to that expected in the SM for each Higgs boson mass considered.

Figure 4 shows the expected and observed limits for $\sigma(p\overline{p} \to H + X)$ relative to the SM for the different Higgs boson masses and the LLR distribution for the 6.7 fb^{-1} of Run II data. So far, no region of the SM Higgs boson mass range can be excluded and no significant excess of events is observed in data. However using the data of DØ alone the sensitivity of the current analysis has reached an expected confidence level for the exclusion of the SM cross section for an Higgs boson with $M_H \approx 165$ GeV close to 85%. With increased integrated luminosity it will be possible to exclude the presence of a Higgs boson with masses around 165 GeV.

[1] R. Barate *et al.*, Phys. Lett. B **565**, 61 (2003).

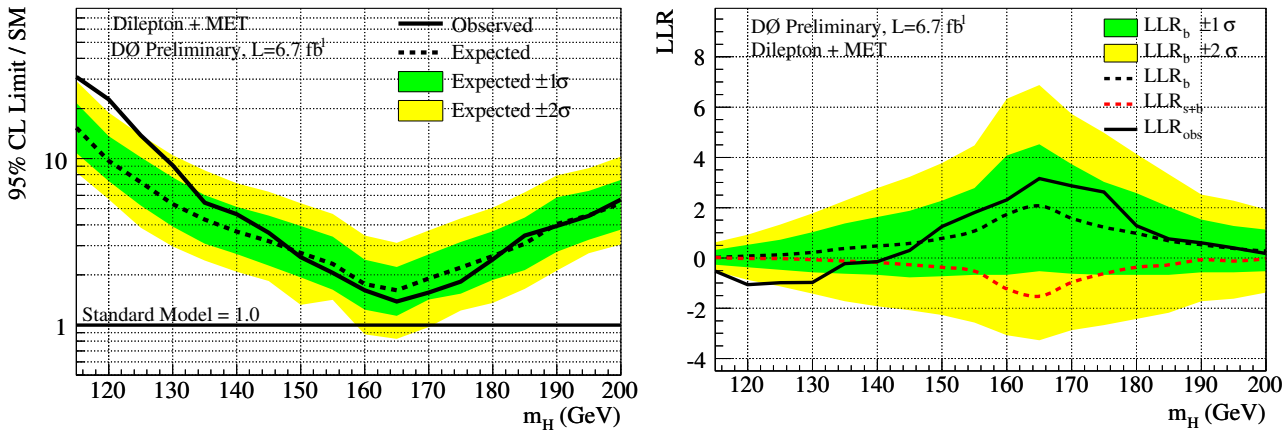

FIG. 4: Excluded cross section ($\sigma(p\overline{p} \to H + X)$) at 95% C.L. in units of the SM cross section (left) and LLR (right) for all three jet multiplicities combined as a function of the Higgs boson mass, using 6.7 fb^{-1} of Run II data.

[2] CDF and DØ Collaborations, T. Aaltonen *et al.*, Phys. Rev. Lett.104, 061802 (2010).
[3] The LEP Electroweak Working Group, the Tevatron Electroweak Working Group, *Precision Electroweak Measurements and Constraints on the Standard Model*, arXiv:0811.4682 [hep-ex].
[4] T. Han, A. Turcot, R-J. Zhang, Phys. Rev. D **59**, 093001 (1999).
[5] M. Carena *et al.* [Higgs Working Group Collaboration], "Report of the Tevatron Higgs working group", hep-ph/0010338.
[6] DØ Collaboration, V. Abazov *et al.*, Phys. Rev. Lett. 96, 011801 (2006).
[7] DØ Collaboration, V. Abazov *et al.*, Phys. Rev. Lett. 104, 061804 (2010).
[8] DØ Collaboration, V. Abazov *et al.*, Nucl. Instrum. Methods Phys. Res. A. **565**, 463 (2006).
[9] T. Andeen *et al.*, Report. No. FERMILAB–TM–2365 (2007).
[10] T. Sjöstrand *et al.*, Comp. Phys. Comm. **135**, 238 (2001), we use version 6.323 or later.
[11] M.L. Mangano, M. Moretti, F. Piccinini, R. Pittau, A. Polosa, JHEP **0307**, 001 (2003), we use version 2.11.
[12] J. Pumplin et al., JHEP **07**, 012 (2002).
[13] R. Brun and F. Carminati, CERN Program Library Long Writeup W5013, 1993 (unpublished).
[14] S. Catani, D. de Florian, M. Grazzini and P. Nason, JHEP **0307**, 028 (2003).
[15] K.A. Assamagan *et al.*, [Higgs Working Group Collaboration], arXiv:hep-ph/0406152.
[16] U. Aglietti, R. Bonciani, G. Degrassi, A. Vicini, arXiv:hep-ph/0610033.
[17] C. Anastasiou, R. Boughezal, F. Petriello, arXiv:0811.3458 [hep-ph].
[18] S. Frixione and B.R. Webber, JHEP **0206**, 029 (2002).
[19] R. Hamberg, W.L. van Neerven, and T. Matsuura, Nucl. Phys. **B359**, 343 (1991) [Erratum-ibid. **B644**, 403 (2002)].
[20] DØ Collaboration, V. Abazov *et al.*, Phys. Rev. Lett. 100, 102002 (2008)
[21] K. Melnikov and F. Petriello, Phys. Rev. D**74**, 114017 (2006).
[22] S. Moch, P. Uwer, Phys. Rev. D**78**, 034003 (2008), we use $\sigma(t\bar{t}) = 7.88$ pb.
[23] J. M. Campbell and R. K. Ellis, Phys. Rev. D **60**, 113006 (1999), we use $\sigma(WW) = 11.66$ pb, $\sigma(WZ) = 3.45$ pb and $\sigma(ZZ) = 1.37$ pb.
[24] T. Gleisberg, S. Höche, F. Krauss, A. Schälicke, S. Schumann and J. Winter, JHEP **0402**, 056 (2004).
[25] T. Binoth, M. Ciccoli, N. Kauer, M. Krämer, JHEP **0503**, 065 (2005), JHEP **0612**, 046 (2006).
[26] T. Junk, Nucl. Instrum. Methods Phys. Res. A. **434**, 435 (1999). A. Read, CERN 2000-005 (30 May 2000).
[27] W. Fisher, FERMILAB-TM-2386-E.
[28] DØ Collaboration, DØ note 5871, http://www-d0.fnal.gov/Run2Physics/WWW/results/prelim/HIGGS/H68/H68.pdf